

Transient study of droplet oscillation characteristics driven by an electric field

Yan-Fei Gao(高燕飞), Wei-Feng He(何纬峰), Adam Abdalazeem, Qi-Le Shi(施其乐), Ji-Rong Zhang(张继荣), Peng-Fei Su(苏鹏飞), Si-Yong Yu(俞思涌), Zhao-Hui Yao(姚照辉), and Dong Han(韩东)
Citation: Chin. Phys. B, 2023, 32 (**12**): 128201. DOI: 10.1088/1674-1056/accd47
Journal homepage: http://cpb.iphy.ac.cn; http://iopscience.iop.org/cpb

What follows is a list of articles you may be interested in

Hydrodynamic binary coalescence of droplets under air flow in a hydrophobic microchannel

Chao Wang(王超), Chao-qun Shen(沈超群), Su-chen Wu(吴苏晨), Xiang-dong Liu(刘向东), Fang-ping Tang(汤方平)
Chin. Phys. B, 2019, 28 (**2**): 024702. DOI: 10.1088/1674-1056/28/2/024702

Novel Fe_3O_4@SiO_2@Ag@Ni trepang-like nanocomposites: High-efficiency and magnetic recyclable catalysts for organic dye degradation

Chao Li(李超), Jun-Jie Sun(孙俊杰), Duo Chen(陈铎), Guang-Bing Han(韩广兵), Shu-Yun Yu(于淑云), Shi-Shou Kang(康仕寿), Liang-Mo Mei(梅良模)
Chin. Phys. B, 2016, 25 (**8**): 088201. DOI: 10.1088/1674-1056/25/8/088201

A theoretical exploration of the influencing factors for surface potential

Liu Xin-Min (刘新敏), Yang Gang (杨刚), Li Hang (李航), Tian Rui (田锐), Li Rui (李睿), Ding Wu-Quan (丁武泉), Yuan Ruo (袁若)
Chin. Phys. B, 2015, 24 (**6**): 068202. DOI: 10.1088/1674-1056/24/6/068202

Contact angle hysteresis in electrowetting on dielectric

Zhao Rui (赵瑞), Liu Qi-Chao (刘启超), Wang Ping (王评), Liang Zhong-Cheng (梁忠诚)
Chin. Phys. B, 2015, 24 (**8**): 086801. DOI: 10.1088/1674-1056/24/8/086801

Transient study of droplet oscillation characteristics driven by an electric field

Yan-Fei Gao(高燕飞)[1], Wei-Feng He(何纬峰)[1,†], Adam Abdalazeem[1], Qi-Le Shi(施其乐)[1], Ji-Rong Zhang(张继荣)[1], Peng-Fei Su(苏鹏飞)[2], Si-Yong Yu(俞思涌)[1], Zhao-Hui Yao(姚照辉)[1], and Dong Han(韩东)[1]

[1] *Advanced Energy Conservation Research Group (AECRG), College of Energy and Power Engineering, Nanjing University of Aeronautics and Astronautics, Nanjing* 210016, *China*
[2] *Dongfang Turbine Co., Ltd, Deyang* 618000, *China*

(Received 12 December 2022; revised manuscript received 28 March 2023; accepted manuscript online 16 April 2023)

Electrowetting technology, a microfluidic technology, has attracted more and more attention in recent years and has broad prospects in terms of microdroplet drive. In this paper, the dynamic contact angle theory is used to develop a numerical model to predict the droplet dynamic contact behavior and internal flow field under electrowetting. In particular, based on the established computational model of droplet force balance, the dynamic process of a droplet under electrowetting is analyzed, including the perspective of pressure variation and force balance inside the droplet. The results show that when the alternating current frequency increases from 50 Hz to 500 Hz, the amplitude of the oscillation waveform after droplet stabilization is 0.036 mm, 0.016 mm, 0.013 mm and 0.002 mm, while the relevant droplet oscillation period T is 11 ms, 4 ms, 2 ms and 1 ms, respectively. It is also found that the initial phase angle does not affect the droplet oscillation amplitude. In addition, the pressure on the droplet surface under alternating current electrowetting increases rapidly to the maximum value with resonant waveform oscillation, and the droplet will present different resonance modes under voltage stimulation. The higher the resonance mode is, the smaller the droplet oscillation amplitude is and the streamline at the interface will present an eddy current, in which the number of vortices matches the resonance mode. A high resonance mode corresponds to a small droplet amplitude, while there are more vortices with a smaller size.

Keywords: electrowetting, dynamic contact angle, level set model, droplet oscillation

PACS: 82.65.+r **DOI:** 10.1088/1674-1056/accd47

1. Introduction

As widespread phenomena in various industrial fields (such as electrostatic spraying,[1] electric demulsification[2] and microfluidics[3]), droplet deformation, breakage and movement in an electric field have always been important areas of research. In particular, the wettability of droplets on solid surfaces has attracted much attention in the fields of microfluidics and heat transfer.

The deformation, movement and wettability of droplets in an electric field are affected by many factors such as droplet location, quantity, diameter, electric field intensity, electric field frequency, fluid physical properties, surfactant and fluid type.[4] The wettability of droplets on a solid surface changes under the electric field; this is called the electrowetting phenomenon.[5] After years of development, electrowetting has been able to realize the transport of droplets between the control electrodes,[6] the directional transport of droplets in the oil phase[7] and the directional transport of underwater oil droplets.[8] Through electrowetting, droplet drive can be realized on a changing two-dimensional array electrode or surface, for example, separation, merging, mixing and transportation. Due to the advantages of in situ control, fast response, flexible manipulation and low energy consumption, electrowetting technology has been widely used in fields of microfluidics such as optics, displays, chip laboratories, printing and separation.[9]

Some scholars have conducted many experiments and theoretical studies on electrowetting to understand how droplets interact with a solid surface under the influence of electric fields. Moreover, in recent years the study of electrowetting phenomena has begun to shift from surface characteristics to the internal mechanism. Zhang *et al.*[10] used a DC piezoelectric voltage to drive an electrowetting system to reduce the sliding resistance at a solid–liquid interface. The friction and slip behavior of the solid–liquid interface on a rough surface under the applied voltage was investigated. The results showed that the unstable region of rough slip behavior of droplets on the surface cannot be explained by the electrowetting equation. He *et al.*[11] studied the wetting and dewetting behavior of nanodroplets with different molecular numbers on the surface of a nano-column array. The scale effect was tested by molecular dynamics (MD) simulation with or without an applied electric field. Ahmad *et al.*[12] reported numerical simulations and experiments on electrowetting-induced oscillatory droplets under different hydrophobic conditions, a phase-field based code with a dynamic contact angle model was used to study the droplet dynamics. Hydrophobicity of the substrate intensified the deformation and internal flow structures of the

†Corresponding author. E-mail: wfhe@nuaa.edu.cn
© 2023 Chinese Physical Society and IOP Publishing Ltd

oscillating droplet. It also influenced the phase difference between the contact angle and the contact radius, producing three different phase regimes. The amplitude and frequency of the droplet oscillation change differently with the surface wettability in different phase regimes. Ko *et al.*[13] observed hydrodynamic flow in droplets using an AC voltage from a configuration with air as the ambient phase. The flow was observed using a laser sheet and fluorescent tracers, and a toroidal vortex flow was reported. Furthermore, droplet oscillations were simultaneously observed and it was explained that the toroidal flow originates from such oscillations. Zhang *et al.*[14] used a DC piezoswing voltage to drive the electrowetting system to reduce the slip resistance of the solid–liquid interface. The results of experimental and theoretical analysis showed that with increase in the piezoswing rate, the slip amplitude of the contact line under electrowetting greatly increased while the corresponding slip frequency decreased. Kang *et al.*[15] found that under probe-type electrowetting there is vortex flow in the droplet, and this vortex flow changes direction with the frequency of applied voltage. Zhang *et al.*[16] conducted an MD simulation to study the static and dynamic wetting of water nanodroplets on the surface of nanostructures in the presence of a vertical electric field. Andreas *et al.*[17] studied the influence of parameters such as density, viscosity and mass on the electrowetting oscillation process and gave the simulation results; it turned out that only electrical grounding from below leads to utilizable oscillations. Markodimitrakis *et al.*[18] used experiments to prove and calculate the influence of the elasticity and thickness of the medium on the beginning of antenna saturation. The results show that the elastic effect is very important, especially when the thickness of the dielectric layer is less than 10 μm; for thicknesses greater than 20 μm the elastic effect is negligible. They attributed this finding to the effect of dielectric thickness on the electric field as well as the distribution of induced electrical stress near the three-phase contact line (TCL). Malk *et al.*[19] dealt with a characteristic hydrodynamic flow appearing in droplets actuated by electrowetting-on-dielectric (EWOD) with an AC voltage. In the coplanar electrode configuration, two pairs of vortex flows were observed to form in a droplet centered on the electrode gap. At the same time, droplet oscillations induced by AC EWOD were also revealed under stroboscopic lighting. These experiments show that vortex location can be controlled by frequency actuation with a fair degree of reproducibility.

Based on the droplet dynamics, we can conclude that revealing the dynamic contact behavior and internal flow mechanism of the electrowetting process is essential for the performance prediction and design of advanced electrowetting devices. The effects of droplet physical characteristics,[17] electric field magnitude,[17,18] polarity[10,14] and wall hydrophobicity[12,13] on the electrowetting phenomenon under DC or AC electric fields have been extensively studied. However, the internal flow field mechanism of droplets under alternating current electrowetting (ACEW), as well as the effects of voltage frequency and initial phase angle on the dynamic contact behavior of droplets, have not been thoroughly and completely investigated. Meanwhile, the connection between physical parameters such as pressure, kinetic energy and force on droplets under ACEW and the oscillation process has not been looked at so far. To better simulate the variation of droplet contact angle, an axisymmetric model and dynamic contact angle theory are introduced in this paper. In addition, a transient numerical model of the force on the droplet is also proposed, and the variation of the droplet surface pressure is obtained. The dynamic contact behavior of droplets and the mechanism of variation of the internal flow field are first looked at from a new perspective by analyzing the force and pressure variation on droplets. Furthermore, the intrinsic connection between change in droplet kinetic energy and droplet oscillation is investigated, and the relationship between droplet velocity, energy and kinetic energy is analyzed. The proposed dynamic contact behavior and internal flow field changes of droplets under different environments provide theoretical support for the subsequent electrowetting research.

2. Numerical models and solution methods

2.1. Dynamic contact angle model

The present work explores the electrowetting effect of a sessile droplet on a solid surface coated with a hydrophobic dielectric material. The basic principle of electrowetting on a medium is shown in Fig. 1. In the electrowetting process the surface of the plate is usually coated with a dielectric layer to prevent electrolysis of the droplet under high voltage. In the same way a hydrophobic layer is applied to the dielectric layer to increase the hydrophobicity of the wall surface,[20] in order to increase the ability to change the contact angle: $\theta_{s,OFF}$ is the contact angle when no electric field is applied and $\theta_{s,ON}$ is the contact angle when an electric field is applied. The surface tensions between solid/liquid, liquid/gas and solid/gas are denoted by σ_{SL}, σ_{LG} and σ_{SG}, respectively.

The surface tension between solid/liquid can be expressed by the Young equation

$$\sigma_{SL}(\mathrm{OFF}) = \sigma_{SG} - \sigma_{LG}\cos\theta_{s,OFF}. \tag{1}$$

The influence of applied voltage (V) on surface tension can be expressed by Lippmann's formula[21]

$$\sigma_{SL}(\mathrm{ON}) = \sigma_{SL}(\mathrm{OFF}) - \frac{1}{2}\left(\frac{\varepsilon_0\varepsilon_d}{d}\right)V^2. \tag{2}$$

From Eqs. (1) and (2) we can get

$$\cos\theta_{s,ON} = \cos\theta_{s,OFF} + [\varepsilon_0\varepsilon_d/(2\sigma_{LG}d)]\,V^2, \tag{3}$$

where ε_0, ε_d and d are the vacuum dielectric constant, dielectric constant and dielectric layer thickness, respectively. Formula (3) represents the contact angle of the droplet under an electric field with applied voltage ($\theta_{s,ON}$).

In electrowetting, an electric field force ($F_e = \varepsilon_0\varepsilon_d V^2/(2d)$) drives the droplet along the TCL, friction resistance (F_f) and packing medium resistance (F_D) as forward resistance. Considering a droplet as an unbounded sphere moving in air, its drag force is calculated as $F_D = 0.5C_D A_D \rho_f U^2$, where C_D, A_D, ρ_f and U denote the drag coefficient, projected area, air density and droplet velocity, respectively.[13] According to the observation of Oprins *et al.*,[22] it is found that when air is the filling medium the resistance can be ignored.

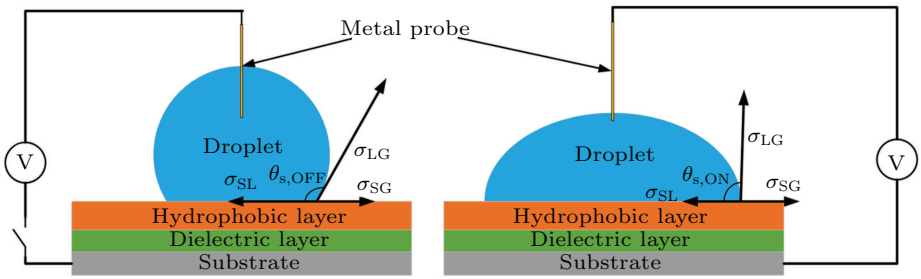


Fig. 1. Schematic diagram of the principle of electrowetting on a medium.

The imbalance of electric field force and friction force will cause acceleration on the contact line. Since the mass near the contact line is very small, the force generated by acceleration is not considered in deriving the dynamic contact angle. Thus, the resultant force (F_{net}) of the oscillating droplet along the TCL direction can be written as

$$F_{net} = F_e - F_f, \tag{4}$$

$$\sigma_{LG}(\cos\theta_{s,D} - \cos\theta_{s,OFF}) = F_e - f_{cl}U_{cl}. \tag{5}$$

Thus, the final expression for the instantaneous dynamic contact angle under electrowetting with voltage V can be written as[14]

$$\theta_{s,D} = \cos^{-1}\left[\cos\theta_{s,OFF} + [\varepsilon_0\varepsilon_d/(2\sigma_{LG}d)]V^2 - (f_{cl}U_{cl}/\sigma_{LG})\right]. \tag{6}$$

Due to the singularity of the droplet at the contact line, obtaining an accurate contact linear velocity $U_{cl}(t)$ is a challenge. If the wall is set as a no-slip boundary, the contact line cannot move. In reality, however, the contact line does move, resulting in infinite viscous shear forces and divergent drag on the wall. To avoid this, the Navier sliding boundary condition ($u_{slip} = \beta\partial u/\partial y$) is introduced to represent the contact line motion as a slip, where β is the slip length, i.e., the distance from the boundary, where the velocity of linear extrapolation will reach zero. In addition, since the model is an axisymmetric regular geometry model, the contact linear velocity in Eq. (6) can be estimated as the rate of change of the droplet contact radius, which is given by[23]

$$U_{cl} = \mathrm{d}R/\mathrm{d}t, \tag{7}$$

where R is the radius of the droplet-wetting area.

Moreover, when the friction law on the contact line is linear, the friction coefficient f_{cl} depends on the tension interaction on the contact line, which has the same units as the viscosity and can be measured from experiments or molecular dynamics simulations. Meanwhile, Cheng *et al.*[24] showed that the larger the slip length, the smaller the obstruction effect of the wall on the fluid. The wall resistance characteristics can be changed by adjusting the slip length.

2.2. Numerical model

2.2.1. Computational domain and boundary conditions

In this paper, the numerical research is carried out in a two-dimensional axisymmetric computational domain. As shown in Fig. 2(a), the droplet is assumed to be deionized water, the ambient medium is air and both the droplet and air are incompressible fluids. Layer 1 is the dielectric layer with a hydrophobic layer; layer 2 is the negative electrode and the probe is the positive electrode. Since the probe is very thin, it has little influence on the droplet flow field and is ignored in the calculation domain. After a voltage is applied, negative charges accumulate on the surface of layer 2 and positive charges accumulate on the surface of layer 1 inside the droplet; the closer to the TCL, the greater the density of positive charges accumulated on the surface of layer 2. An electric field is formed between the positive and negative charges, which disturbs the droplet. At the initial time, the droplet velocity is 0, and the air condition outside the droplet is atmospheric pressure. The droplet interface is tracked by the level set variable (ϕ), where the droplet has a value of ϕ equal to 1 and the surrounding air has a value of ϕ equal to 0. In addition, the numerical calculations are based on the following assumptions:

(a) The shape of the droplet is assumed to be a spherical cap.

(b) The voltage drop along the working fluid is ignored, thus, the droplet is assumed to be a conductor.

(c) The effect of surfactants or any other foreign particles on deionized water is not considered.

The mathematical model assumes that the fluid is laminar and incompressible. The laminar Navier–Stokes equations are established for droplet and air, respectively, and the effect of surface tension of the droplet is considered.[25]

In the simulation of axisymmetric droplet diffusion, several boundary conditions are set to restore the actual scenario. S1 is the symmetric boundary, S2 is set as the wetted wall and S3 is set as the open boundary, so that the model converges by changing the system pressure release when the droplet moves. To accurately capture the influence of the stress tensor on the droplet, the mesh and wetting wall boundary near the droplet surface are specially refined, as shown in Fig. 2(b). The final calculation results pass the grid independence numerical test, and the total number of grids is 14412.

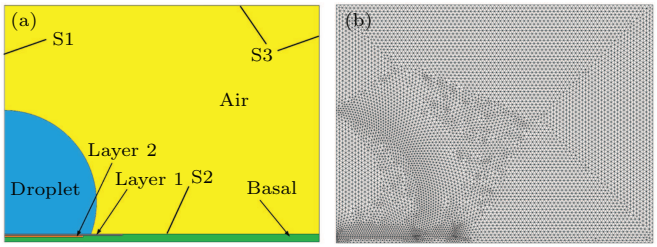


Fig. 2. Geometric model for electrowetting simulation: (a) computational domains and boundary conditions; (b) finite element meshing of the model geometry.

2.2.2. Governing equation

The governing equations in this paper include continuity and momentum equations of level set variables. The details are as follows:

$$\nabla \cdot u = 0, \tag{8}$$

$$\rho \frac{\partial u}{\partial t} + \rho(u \cdot \nabla)u = \nabla \cdot \left[-pI + \mu\left(\nabla u + (\nabla u)^{\mathrm{T}}\right)\right] + \rho g + F_{\mathrm{st}}, \tag{9}$$

where g, p and F_{st} are gravity, pressure and surface tension, respectively.

The level set variable (ϕ) is used to track two phases, where $\phi = 1$ represents the secondary phase (i.e., droplet) and $\phi = 0$ represents the primary phase (i.e., air). Therefore, $\phi = 0.5$ denotes the droplet interface, where the level set variable (ϕ) can be calculated using the following equation:

$$\frac{\partial \phi}{\partial t} + u \cdot \nabla \phi = \gamma \nabla \cdot \left(\varepsilon \nabla \phi - \phi(1-\phi)\frac{\nabla \phi}{|\nabla \phi|}\right), \tag{10}$$

where ε is the interface thickness parameter and γ is the reinitialization parameter, and for numerical calculations the appropriate choice is $\varepsilon = h$, where h is the grid cell size.

The surface tension in Eq. (9) acting on the interface can be calculated by the normal vector of the interface and the curvature of the interface, as shown below:[23]

$$F_{\mathrm{st}} = \sigma k \delta \boldsymbol{n} + \nabla \cdot \left(\sigma\left(I - \left(\boldsymbol{n}\boldsymbol{n}^{\mathrm{T}}\right)\right)\delta\right). \tag{11}$$

The δ function is approximately a smoothing function

$$\delta = 6|\nabla \phi||\phi(1-\phi)|, \tag{12}$$

where σ represents the surface tension coefficient, $\boldsymbol{n}$ represents the unit normal vector at the interface, k represents the curvature of the fluid interface and δ represents the Dirac function.

In addition, the fluid domain is divided into two materials by the interface, and in each subdomain the material properties are constant. However, the density and viscosity are discontinuous throughout the solution domain. To simplify the calculation so that the values of density, viscosity and surface tension can continuously transition from the air to the droplet, the following formula is used:[25]

$$\rho = \rho_{\mathrm{g}} + \left(\rho_{\mathrm{l}} - \rho_{\mathrm{g}}\right)\phi, \tag{13}$$

$$\mu = \mu_{\mathrm{g}} + \left(\mu_{\mathrm{l}} - \mu_{\mathrm{g}}\right)\phi, \tag{14}$$

where the subscripts g and l represent the gas and liquid, μ_{l} and μ_{g} indicate the dynamic viscosity of droplet and air, and ρ_{l} and ρ_{g} indicate the density of droplet and air, respectively.

2.3. Model validation

The friction coefficient f_{cl} can be measured by fitting molecular dynamics simulation data to experimental data. In general, when contact angle hysteresis is not considered, it is found that the larger values ($f_{\mathrm{cl}} = 0.2$–0.4 N·s·m^{-2}) fit the experimental data well,[26–28] otherwise a smaller value ($f_{\mathrm{cl}} = 0.18$ N·s·m^{-2}) is more suitable.[29,30] In order to verify the correctness and accuracy of the model constructed in this paper, other materials have the same characteristics under the same voltage (32 V DC) (see Table 1). In the simulation in this article, $f_{\mathrm{cl}} = 0.1$ N·s·m^{-2} and $f_{\mathrm{cl}} = 0.15$ N·s·m^{-2} are used, as shown in Fig. 3. When β =0.3 μm and $f_{\mathrm{cl}} = 0.1$ N·s·m^{-2}, molecular dynamics simulation results data more accurately predict the experimental data of Cheng *et al.*[24] The data obtained from the numerical simulation are basically consistent with the experimental data, and the error of the data is very small, which indicates the correctness of the model. Therefore this article chooses $\beta = 0.3$ μm and $f_{\mathrm{cl}} = 0.1$ N·s·m^{-2} for subsequent simulation.

Table 1. Material properties of liquids/substrates used in direct current electrowetting experiments and simulations.

ρ (kg·m^{-3})	μ (Pa·s)	σ_{LG} (N·m^{-1})	$\theta_{\mathrm{s,OFF}}$ (°)	ε_{d} (F·m^{-1})	Volume (μl)	d (m)
997	1.001×10^{-3}	7.275×10^{-2}	118	3.9	5	5×10^{-7}

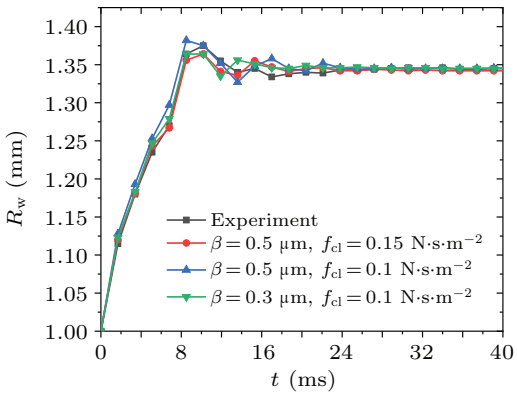


Fig. 3. Comparison of experimental and numerical results at different times when the static contact angle is 118°.

2.4. Force analysis model

By analyzing the force balance of the droplet under electrowetting, the relationship between the force change and other parameters of the droplet can be obtained. Cheng *et al.*[24] observed that viscous dissipation is not obvious in droplet oscillation dynamics with an AC electric field. In addition, Ahmad *et al.*[14] observed that the viscous force is negligible compared with the applied electricity and friction. Therefore, the influence of viscous force is ignored in this model. In the process of droplet oscillation, the friction force $F_f = f_{cl}U_{cl}$ on the contact line during the oscillation of the droplet is the main part of the resistance. Therefore, F_f acts as a resistance to the electric field force in the mechanical analysis. In the process of droplet oscillation under electrowetting, droplet motion starts from the TCL. Therefore, in the force balance analysis, the dominant force along the TCL ignores other forces in the vertical direction.

The applied sinusoidal waveform voltage (V) is given by

$$V = V_0 \sin(2\pi ft + \varphi). \tag{15}$$

Therefore, the field forces F_e are as follows:

$$\begin{aligned} F_e &= \varepsilon_0\varepsilon_d V^2/(2d) = (\varepsilon_0\varepsilon_d/(2d))V_0^2[\sin(2\pi ft+\varphi)]^2 \\ &= KV_0^2[\sin(2\pi ft+\varphi)]^2, \end{aligned} \tag{16}$$

where $K = \varepsilon_0\varepsilon_d/(2d)$.

3. Results and analysis

In the simulation calculation, the droplet volume is 5 μl. The initial shape of the droplet is a spherical crown, and the initial contact angle is 110°. The total thickness of the dielectric and hydrophobic layer d =2.5 μm and the total effective relative dielectric constant ε_d = 2.8, The droplet is deionized water, with $\rho = 997$ kg·m^{-3} and kinematic viscosity $\mu = 1.01 \times 10^{-3}$ Pa·s. The ambient gas is air, and the droplet is in an equilibrium state before the voltage is applied ($t = 0$ ms).

3.1. Dynamic contact characteristics of droplets under ACEW

Figure 4 shows the variation of droplet contact radius with time, where R_w is the wetting radius of the droplet. The amplitude of the droplet is the displacement of the droplet contact line moving forward along the wall during diffusion, and is represented by the symbol A_m. After completion of the first oscillation, the droplet maintains a new contact radius higher than the initial contact radius and continues to oscillate with the maximum possible diffusion; then, the time it takes to return to the original contact radius during a certain period of oscillation is called the stable oscillation period T. As can be seen from Fig. 4, the variation of the displacement R_w of the droplet contact line tends to be a sinusoidal waveform. The AC amplitude is kept constant, and its magnitude is 75 V. When the AC frequency increases from 50 Hz to 500 Hz, the oscillating wave amplitudes after the droplet stabilization are 0.036 mm, 0.016 mm, 0.013 mm and 0.002 mm, respectively, and the oscillation periods T of the droplet wetting radius are 11 ms, 4 ms, 2 ms and 1 ms, respectively. It can be seen that with the increase in AC frequency, the stable oscillation period of the droplet decreases stepwise, and the amplitude of the stable waveform after oscillation also decreases stepwise. It can be seen from the analysis that the surface of the droplet under stimulation with different frequencies presents different surface waves, which causes the movement of the contact line.

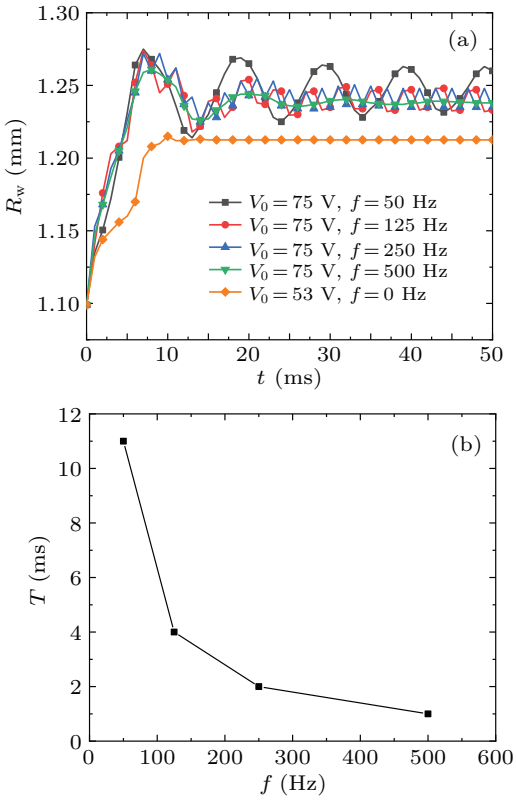


Fig. 4. Dynamics of droplets under ACEW with time. (a) Variation of droplet wetting radius with time at different frequencies. (b) Oscillation period of droplet wetting radius at different frequencies.

In fact, there is a delay between the movement of the droplet contact line and the change in the electric field force. The higher the AC frequency is, the faster the rate of change the electric field force will be: if the electric field force changes too fast, it will hinder the process of droplet contact wire movement, which shows that the larger the AC frequency is, the smaller the oscillation amplitude of the droplet is. It can be seen from Fig. 4(a) that when $f = 500$ Hz, the droplet oscillation amplitude is very small, which is similar to the variation trend of droplet wetting radius under direct current electrowetting (the DC voltage is the effective value corresponding to the AC amplitude).

Figure 5 shows the time variation of different forces (electric field force F_e, contact line friction F_f and net force F_{net}) on the droplet at $V_0 = 75$ V, $f = 50$ Hz and $\varphi = 0°$. As shown in Fig. 5, the line of contact friction $F_f = f_{cl}U_{cl}$, the line of contact friction force and the direction depend on the value of the linear velocity. The speed changes along the sine wave, so the line of contact friction also presents a sinusoidal waveform change, with the positive and negative friction corresponding to expanding and contracting behavior of the contact wires. As shown in Fig. 4(a), within $t = 0$–6 ms, the droplet amplitude rapidly increases to a peak, and after $t = 6$ ms, the droplet amplitude presents a waveform oscillation, corresponding to Fig. 5. The droplet velocity reaches its maximum at the initial time, the contact line friction reaches its maximum and then the droplet size presents waveform fluctuation. As Ahmad *et al.*[12] mentioned, the magnitude and direction of friction depend on the speed of the contact line. The positive and negative values of friction represent the diffusion stage and the contraction stage, respectively. Friction increases with time, and reaches a maximum when the electric field force reaches a peak. At the same time, it is accompanied by the maximum change in diffusion radius. In addition, the static F_{net} size near the droplet contact line in Fig. 5 also changes with a waveform oscillation, which further explains that the variation curve of stable droplet oscillation amplitude under the action of electrowetting is a sinusoidal waveform.

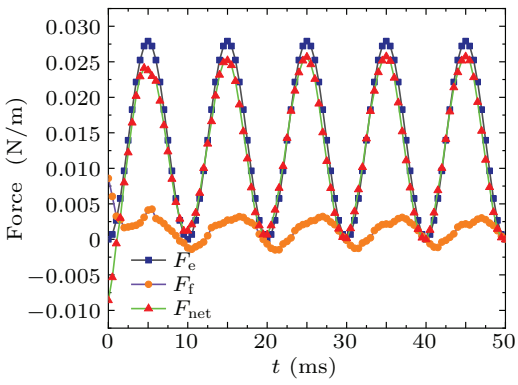


Fig. 5. Change of force on the contact line with time ($V_0 = 75$ V, $f = 50$ Hz, $\varphi = 0°$).

Figure 6 shows the change in droplet contact behavior over time when the AC voltage is the same and the initial phase angle is different. As can be seen from Fig. 6, when the initial phase angle is 0°, 45° or 90° there is no significant difference in the droplet wetting radius, indicating that the initial phase angle does not affect the change in the droplet wetting radius. However, the initial phase angle is related to the initial phase angle of the droplet oscillation curve. For $\varphi = 45°$, 0° and 90°, the droplet reaches stable oscillation successively and then continues to move with the same stable oscillation period.

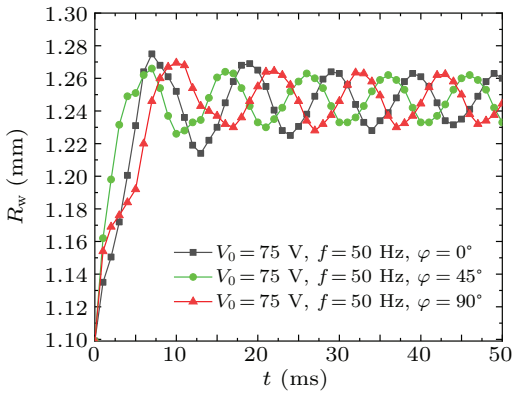


Fig. 6. Change of droplet contact radius under different phase angles.

3.2. Droplet internal flow under ACEW

Under the action of an electric field force, the contact angle of stationary droplets changes, as shown in Fig. 4(a). The droplet presents a sinusoidal oscillation motion along the wall. It can be seen that under the effect of electrowetting, the static internal flow of the droplet is changed into an internal eddy current under the stimulation of an electric field. Figure 7 shows the changes in the average pressure at the gas–liquid surface with time at different frequencies. It can be seen from Fig. 7 that under AC stimulation, the pressure at the interface rapidly increases from close to atmospheric pressure to the maximum pressure value, and then the interface pressure changes to show waveforms. The reason for the pressure change can be obtained by referring to the change in the droplet contact radius over time in Fig. 4(a). In the initial

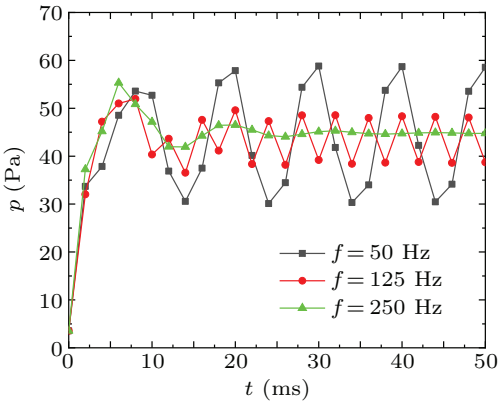


Fig. 7. Change of average pressure at the gas–liquid interface with time.

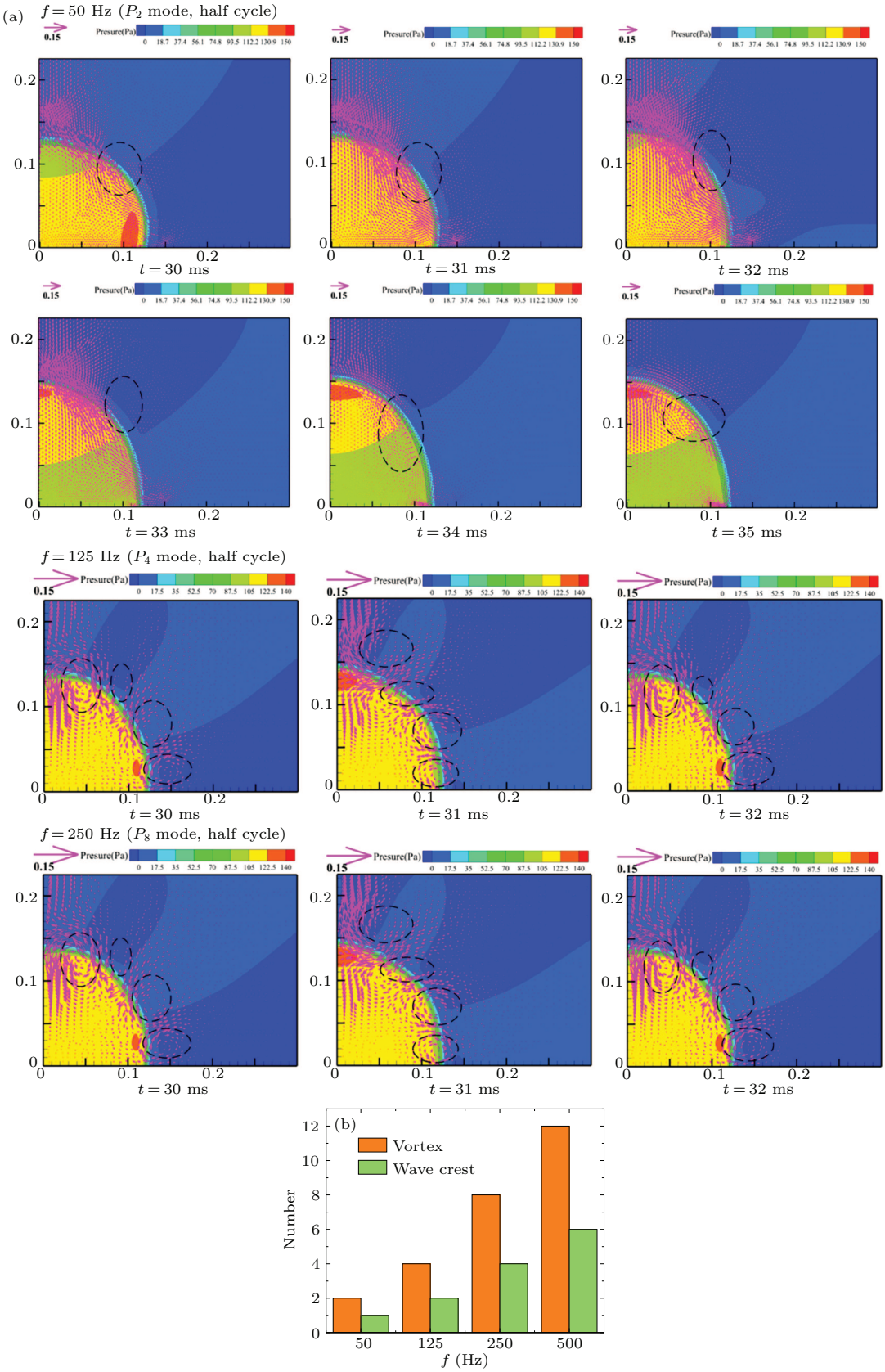


Fig. 8. The change of droplet morphology with different frequency. (a) Internal flow field variation. (b) Vortex and wave crest relationship diagram.

deformation stage of the droplet, the force balance of the droplet is broken under the stimulation of the electric field force, and a certain kinetic energy is accumulated, which eventually leads to the accumulation of pressure at the edge of the droplet. Under the action of pressure, the droplet reciprocates, resulting in the accelerated retreat of the contact line and oscillation of the wetting radius. At the same time, since the voltage applied to the droplet constantly changes with time, the pres-

sure near the droplet contact line will also constantly change with the trend of voltage variation. In addition, the larger the frequency f is, the smaller the accumulated pressure oscillation amplitude at the interface will be. The reason for this is that the pressure change has a delay compared with the voltage change. The larger the voltage frequency is, the faster the voltage change will be, so the change of electric field force will also be accelerated. Therefore, an electric field force that changes too quickly will interfere with the pressure accumulation process at the interface. The larger the frequency f is, the stronger the interference will be, and the smaller the eventual change of the interface pressure will be.

Figure 8 shows the change of droplet morphology over time with different frequencies. Figure 8(a) shows the velocity vector field and pressure distribution inside the droplet at different frequencies. In this figure, half an oscillation period is selected for modes P_2 and P_4 and one oscillation period is selected for modes P_8. In the process of droplet oscillation, each peak value of droplet oscillation corresponds to a resonance mode P_n ($n = 2, 4, \ldots$), and the value of n depends on the number of wave peaks at the droplet interface. As can be seen from Fig. 4, the higher the resonance mode is, the smaller the droplet oscillation amplitude is. In addition, the recirculating eddies can be identified from the streamline profile and the number of eddies matches their resonance modes. For example, two vortices can be observed in P_2 mode, four in P_4 mode and eight in P_8 mode, and most of the vortex centers are located on or near the free surface. It is also noted that the oscillation amplitude of the droplet decreases continuously as the frequency f increases from 50 Hz to 250 Hz. As can be seen from Fig. 8(a), the oscillation process of the droplet decreases continuously as the oscillation mode of the droplet changes from mode P_2 to mode P_8, and the size of the vortex at the interface also decreases continuously. As mentioned by Yi *et al.*,[23] when a droplet is actuated under ACEW, the droplet exhibits time-harmonic shape oscillations. The oscillation amplitude is found to decrease with increasing actuation frequency due to the dominant effect of inertia over other forces. The surface wave propagates with a similar phase velocity to capillary waves.

The connection between the droplet surface pressure and the resonance mode can be investigated through Figs. 7 and 8. When $f = 50$ Hz, the pressure changes slowly, so the droplet surface forces change more slowly and can be seen as a more stable oscillation. Due to the slow change of droplet surface perturbation, there are fewer wave peaks and vortices on the surface. At the same time, when $f = 250$ Hz the rate of pressure change is accelerated, so the force balance on the droplet surface changes dramatically. Due to the strong change in perturbation on the droplet surface, the wave and vortex currents on the surface also increase. In addition, the pressure amplitude becomes smaller from $f = 50$ Hz to 250 Hz and the intensity of droplet surface perturbation decreases, resulting in a reduction in the size of wave crests and vortices.

Figure 8(b) shows the quantitative correlation between the number of vortices n on the droplet surface and the number of wave peaks w at the interface during the oscillation. Resonance modes are P_2 corresponding to one wave, P_4 to two waves, P_8 to four waves and P_{12} to six waves. It can be concluded from Fig. 8(b) that $w = z/2$, namely, the number of vortices on the droplet surface z is always twice the number of wave peaks, and the interface wave peaks caused by droplet oscillation are always symmetric along the center line. The larger f is, the more frequently the interface is disturbed, but the intensity of the disturbance of the electric field force is decreasing. Therefore, under voltage stimulation, the larger frequency of the droplet the more surface crests and vortices there are and the smaller the size of ripples generated by the droplet surface is.

4. Conclusions

Based on our numerical simulation, the dynamic contact process and internal flow field of droplets under electrowetting are studied in this paper. The following conclusions are drawn.

1. The dynamic contact angle model is used to simulate and predict the electrowetting process more reasonably, and the change in droplet contact radius under different frequencies and initial phase angles is studied. When the AC frequency increases from 50 Hz to 500 Hz, the oscillating wave amplitudes of droplet stabilization are 0.036 mm, 0.016 mm, 0.013 mm and 0.002 mm, respectively, and the oscillation periods T of the droplet wetting radius are 11 ms, 4 ms, 2 ms and 1 ms, respectively. With increase in frequency, the stable oscillation period of the droplet decreases stepwise, and the amplitude of the stable waveform after oscillation also decreases stepwise. In addition, when the initial phase angle is 0°, 45° or 90°, there is no significant difference in the droplet wetting radius, indicating that the initial phase angle does not affect the change in the droplet wetting radius.

2. A model of droplet force variation in the electrowetting process is proposed, and it is concluded that the friction of the contact line presents sinusoidal waveform changes. The positive and negative friction forces, respectively, correspond to the expansion and contraction behaviors of the contact line. The static F_{net} near the droplet contact line also changes as a waveform oscillation, which further explains why the fluctuation curve of stable droplet oscillation amplitude under the action of electrowetting is a sinusoidal waveform.

3. In the case of ACEW, the droplet interface will show velocity vortices and oscillating ripples corresponding to the frequency. As the frequency f increases from 50 Hz to 250 Hz

the oscillation amplitude of the droplet decreases continuously, and the oscillation mode of the droplet changes from P_2 to P_8 mode. The oscillation process of the droplet decreases continuously, and the vortex size at the interface also decreases continuously.

Acknowledgements

The authors expressed their sincere gratitude to the Natural Science Foundation of Jiangsu Province (Grant No. BK2020194), the Basic Research Fund of Central University (Grant No. NS2022026), and the Graduate Research and Practice Innovation Program (Grant No. xcxjh20220215).

References

[1] Gao Q J, Wang Z H and Wang J Q 2006 *Modern Paint & Finishing* 39 (in Chinese)
[2] Zhang J, Dong S P and Gan Q R 2007 *Journal of Chemical Industry and Engineering* 875 (in Chinese)
[3] Link D R, Grasland-Mongrain E, Duri A, Sarrazin F, Cheng Z, Cristobal G, Marquez M and Weitz D A 2006 *Angewandte Chemie International Edition* **45** 2556 (in Chinese)
[4] Wang D B, Wang J F, Huo Y P, Liu H L and Wang X Y 2020 *Journal of University of Chinese Academy of Sciences* **37** 274
[5] Beni G and Hackwood S 1981 *Appl. Phys. Lett.* **38** 207
[6] Pollack M G, Shenderov A D and Fair R B 2002 *Lab Chip* **2** 96
[7] Orli D V, Brain G P and Ketan H B 2003 *Nature* **426** 515
[8] Liu M , Nie F Q, Wei Z, Song Y and Jiang L 2010 *Langmuir the Acs Journal of Surfaces & Colloids* **26** 3993
[9] Dai H, Dong Z and Jiang L 2020 *Chemical Journal of Chinese Universities* **41** 1 (in Chinese)
[10] Zhang Y F, Wang Y N, Tang C, Zhou G Y, Yu J X, He H T and Qi H M 2020 *Tribology International* **106** 128
[11] He X, Wang Y F, Zhang B X, Wang S L, Yang Y R, Wang X D and Lee D J 2021 *Langmuir* **37** 14571
[12] Israr A, Manabendra P and Khan M K 2022 *Journal of Molecular Liquids* **353** 118
[13] Zhang Y F, Wang Y N, Tang C, Zhou G Y, Yu J X, He H T and Qi H M 2020 *Colloids and Surfaces A Physico-chemical and Engineering Aspects* **602** 125075
[14] Kang, Hyoung K 2002 *Langmuir* **18** 10318
[15] Hong J S, Ko S H, Kang K H and Kang I S 2008 *Microfluid Nanofluid* **5** 263
[16] Zhang B X, Wang S L, He X, Yang Y R and Wang X D 2021 *Journal of Molecular Liquids* **1** 116039
[17] Andreas T, Thomas V B, Stefan C, Bernhard M and Bernhard J 2019 *IEEE Sensors Journal* **19** 1379
[18] Markodimitrakis Ioannis E, Sema Dionysios G, Chamakos Nikolaos T, Papadopoulos Periklis and Papathanasiou Athanasios G 2021 *Soft Matter* **17** 4335
[19] Malk R, Fouillet Y and Davoust L 2011 *Sensors and Actuators B: Chemical* **154** 191
[20] Hong F J and Zheng P 2010 *Journal of Engineering Thermophysics* **31** 1205 (in Chinese)
[21] Lippmann G 1875 *Ann. Chim. Phys* **5** 494
[22] Oprins H, Bart V and Martine B 2012 *Micromachines* **3** 150
[23] Yi L, Sur A, Pascente C, Ravi Annapragada S, Ruchhoeft P and Liu D 2017 *International Journal of Heat & Mass Transfer* **106** 920
[24] Cheng Y L, Jiang Y and Xue Z P 2017 *Journal of Engineering Thermophysics* **38** 7 (in Chinese)
[25] Tian L 2015 *Numerical simulation of oscillation of drops using level set method* (Hengyang: University of South China) (in Chinese)
[26] Decamps C and De Coninck J 2000 *Langmuir* **16** 10150
[27] Annapragada S R, Dash S, Garimella Suresh V and Murthy Jayathi Y 2011 *Langmuir* **27** 8198
[28] Wang K L and Jones T B 2005 *Langmuir* **21** 4211
[29] Oh J M, Ko S H and Kang K H 2010 *Physics of Fluids* **22** 032002
[30] Hong J, Kim Y K, Kang K H, Kim J and Lee S J 2014 *Sensors & Actuators: B. Chemical* **190** 48